Available online at www.sciencedirect.com
SCIENCE DIRECT®
International Journal of Heat and Mass Transfer 48 (2005) 1633–1646
International Journal of HEAT and MASS TRANSFER
www.elsevier.com/locate/ijhmt

Transient modeling of micro-grooved heat pipe

Balram Suman [a,b,*], Sirshendu De [c], Sunando DasGupta [c,*]

[a] Department of Chemical Engineering and Materials Science, Mailbox # 30, 151 Amundson Hall, 421 Washington Ave, SE, University of Minnesota, MN 55455, USA
[b] School of Mathematics, Mailbox # 30, 151 Amundson Hall, 421 Washington Ave, SE, University of Minnesota, MN 55455, USA
[c] Department of Chemical Engineering, Indian Institute of Technology, Kharagpur 721302, India

Received 21 July 2004
Available online 22 December 2004

Abstract

One-dimensional transient model for fluid flow and heat transfer is presented for a micro-grooved heat pipe of any polygonal shape utilizing a macroscopic approach. The coupled non-linear governing equations for the fluid flow, heat and mass transfer are developed based on first principles and are solved simultaneously. The transient behavior for various parameters, e.g. substrate temperature, radius of curvature, liquid velocity, etc. are studied. The effects of the groove dimensions, heat input and Q-profiles on the studied parameters have been evaluated. The steady state profiles for substrate temperature, radius of curvature, liquid velocity etc. have also been generated. The model predicted steady state substrate temperature profile is successfully compared with the experimental results from the previous study. The general nature of the model and the associated parametric study ensure the wide applicability of the model.

Keywords: Micro-grooved heat pipe; Transient modeling; Capillary meniscus; Capillary limit

1. Introduction

Micro-grooved heat pipe is a reliable and efficient heat transport device and is currently an active area of research. The heat pipe has been used in several technologically important processes requiring augmented heat transfer e.g., in the electronic packaging industry, in micro-gravity environments, and spacecraft thermal control because of its high efficiency, reliability and cost effectiveness. It is best described by dividing it into three sections. Heat is input through the evaporative section, vaporizing the coolant liquid. The vapor then passes through the adiabatic to the condenser section. In the condenser section, the vapor releases it latent heat and gets liquefied. The liquid flows towards the evaporative section, due to capillary pumping, generated by the change in the radius of curvature of the liquid meniscus.

Cotter [1] first proposed the concept of micro-heat pipe. That is essentially a wickless heat pipe for the uniform temperature distribution in electronic chips. The flow of fluids inside the pipe is caused by the change in pressure (due to changes in capillary and intermolecular force field) along the length of the heat pipe. The net capillary force is generated by the combined effect of the evaporating and condensing menisci [2]. The flow

* Corresponding authors. Tel.: +1 612 625 6083; fax: +1 612 626 7246 (B. Suman); tel.: +91 3222 283922; fax: +91 3222 255303 (S. DasGupta).
E-mail addresses: suman@cems.umn.edu (B. Suman), sunando@che.iitkgp.ernet.in (S. DasGupta).

0017-9310/$ - see front matter © 2004 Elsevier Ltd. All rights reserved.
doi:10.1016/j.ijheatmasstransfer.2004.11.004

Nomenclature

a	side length of a regular polygon or smaller side of a rectangle, m
a_1	larger side length of a rectangle, m
A_{cs}	area of cross-section of substrate, m^2
A_l	total liquid cross-section area, m^2
A'_l	liquid cross-section area of one corner, m^2
B_1	constant in expression for A_l
B_2	constant in expression for $\frac{dR^*}{dX^*}$ [Eqs. 6 and 11]
C_{pl}	specific heat of the coolant liquid, J/(kg K)
C_{ps}	specific heat capacity of the substrate, J/(kg K)
D_h	hydraulic diameter, m
f	friction factor
g	acceleration due to gravity, m/s^2
K'	constant in expression for B_2
K_s	thermal conductivity, W/(m K)
L	length of heat pipe, m
L_h	half of total wetted length, m
L'_h	half of wetted length for one corner, m
n	number of sides of a polygon
N_{Re}	Reynolds number
P_l	liquid pressure, N/m^2
P^*	non-dimensional liquid pressure
P_R	reference pressure, N/m^2
P_{v_0}	pressure in vapor region, N/m^2
Q	net heat flux supplied to the liquid, W/m^2
Q'	net heat supplied, W
Q_v	heat flux for vaporization of liquid, W/m^2
R	radius of curvature, m
R^*	non-dimensional radius of curvature
R_0	reference radius of curvature, m
R_m	meniscus surface area per unit length, m
t	time, s
t^*	dimensionless time
T_{con}	temperature at the cold end, °C
T_l	temperature of the coolant liquid, °C
T_l^*	dimensionless temperature of the coolant liquid
T_R	reference temperature, °C
T'_{ref}	reference temperature used by Anand et. al. [23]
T_s	temperature of substrate, °C
T_s^*	dimensionless substrate temperature
V_l	axial liquid velocity, m/s
$\lvert V_l \rvert$	magnitude of axial liquid velocity, m/s
V^*	non-dimensional liquid velocity
V_R	reference liquid velocity, m/s
w_b	polygon pitch, m
x	coordinate along the heat pipe, m
X^*	non-dimensional coordinate along heat pipe

Greek symbols

α	half apex angle of polygon, rad
β	inclination of substrate, rad
γ	contact angle, rad
ϕ	curvature, m^{-1}
λ_l	latent heat of vaporization of coolant liquid, J/kg
μ_l	viscosity of coolant liquid, $kg\,m^{-1}\,s^{-1}$
ρ_l	density of coolant liquid, kg/m^3
ρ_s	density of substrate, kg/m^3
σ_l	surface tension of coolant liquid, N/m
τ	time constant, s^{-1}
τ_w	wall shear stress, N/m^2

of fluid is primarily governed by the pressure jump at the interface of the liquid and the vapor. The pressure jump at the interface is a function of the radius of curvature of the liquid meniscus, surface tension and the wettability of the coolant liquid and substrate system [3–12].

Peterson and his co-workers [13,14] have made significant contributions to the related area of heat transfer from small devices. They successfully used the Young–Laplace equation to describe the internal fluid dynamics of such devices. From these studies, it has been concluded that the longitudinal groove design is crucial to increase the heat transport capacity of these miniature devices and the small grooves provide the necessary capillary forces for the liquid to flow back into the evaporative zone. The minimum meniscus radius and maximum heat transport in triangular grooves have also been studied [15]. A detailed thermal analysis and different limitations of a micro-heat pipe have been studied by Khrustalev and Faghri [16]. Xu and Carey [17] developed an analytical model for evaporation from a V-shaped micro-groove surface assuming that the evaporation takes place only from the thin film region of the meniscus. Stephan and Busse [18] have presented a model for the calculation of the radial heat transfer coefficient in heat pipes with open grooves and have shown that the assumption of an interface temperature equal to the saturation temperature of the vapor leads to a large over-prediction of the radial heat transfer coefficient. Ravikumar and DasGupta [19] presented an integrated model of evaporation from V-shaped micro-grooves. Their model incorporates the evaporation from the capillary as well as the transition region of the extended meniscus as a function of groove length. Later, researchers have investigated the concept of using micro-heat

pipe as effective heat spreader [20,21] as well as determination of dry-out length [22,23]. Recently, Cotton and Stores [24] presented one-dimensional semi analytical model for prediction of wetted length, supported by inclined triangular capillary groove. They have used the concept of accommodation theory to account for the change in radius of curvature at the liquid–vapor interface. Suman et al. [25] have presented a generalized steady state model for micro-grooved heat pipe of any polygonal shape.

The study of transient phenomena is important for the startup and shutdown applications and to understand the capillary behavior. The transient behavior of heat pipes under various operating conditions has been under study for quite some time [26–32]. It has been shown that the transient behavior of the heat pipe is affected by the thermal capacity and conductance of the substrate, capillary phenomena and the coolant liquid. Chang and Colwell [26] and Faghri and Chen [27] used two dimensional heat conduction equations for the substrate, which were coupled with the fluid flow. Tounier and El-Genk [28] have taken transient in all transfer processes i.e. heat, mass and momentum. Later, Zhu and Vafai [29] have used transient in heat transfer process and steady state in other transfer processes reasoning that the heat transfer is the slowest process. Most of the transient heat pipe studies carried out so far is for the wicked heat pipe. The potential applicability of micro-grooved heat pipe emphasizes the importance of the study of the unsteady state behavior.

In this work, one-dimensional transient equations are developed for micro-grooved heat pipe. The model developed is capable of handling different operating conditions e.g., any groove geometry, heat flux distribution etc. The coupled non-linear governing equations for the fluid flow, heat and mass transfer under transient condition are solved numerically. The transient behavior of various parameters e.g., substrate temperature, radius of curvature of the liquid meniscus, liquid velocity, liquid pressure, etc. are studied. The effects of the groove geometry, groove dimensions, heat load and Q-profile on the studied parameters have been evaluated. The steady state profiles for substrate temperature, liquid velocity etc. have also been developed. The model predicted steady state substrate temperature profiles have been successfully compared with the results available in the literature.

2. Theory

The micro-grooved heat pipe considered here can be of any polygonal shape. Though the model equations are general in nature and can handle any polygon, an equilateral triangular heat pipe has been studied as a test case. The schematic of the heat pipe is shown in Fig. 1(a). The hot and the cold ends are specified as the farthest end of evaporative and the condenser region, respectively. The heat flux absorbed/released by the liquid from the substrate in the evaporative and condenser regions i.e. Q-profiles are assumed to be either linearly distributed or a constant although the model is capable to handle any type of Q-profiles. Sufficient amount of the coolant liquid is charged to the system so that at the steady state, the grooves at the bottom of the heat pipe i.e., the cold end remains filled with the coolant liquid, such that the radius of curvature can be calculated from the geometry of the system ($R = R_0$).

The model developed simulates the transient fluid flow, heat transfer and relates them to the capillary forces present in the system. The effects of thermal resistance in the coolant liquid and temperature variation are neglected since the thickness of liquid pool is very small. The thermal conductive resistance of the liquid pool will be considerably small compared to the other resistances. This is principally due to the very small thickness of the liquid pool. A representative calculation for the maximum resistance (for the lowest heat input) shows the resistance is approximately 7.5×10^{-4} mK/W, whereas the axial thermal resistance is at least several orders of magnitude higher. The model equations are developed for all three regions i.e., evaporative, adiabatic and condenser encompassing the complete heat pipe. The governing equations are derived under the following assumptions:

(i) One-dimensional unsteady incompressible flow along the length of heat pipe; (ii) uniform distribution of heat input to the solid substrate; (iii) negligible viscous dissipation; (iv) at unsteady state, sensible heat accumulation by the substrate is negligible compared to the heat taken up by the coolant liquid from the substrate; (v) constant pressure in the vapor region in the operating range of temperature. The constant pressure assumption is valid in this case as the vapor flow space in the channels is quite large specially considering the low heat fluxes used in this study. The vapor pressure drop required for flow has been calculated and found to be very small; (vi) one-dimensional temperature variation along the length of heat pipe; (vii) shear stress at the liquid vapor interface has been neglected; (viii) predefined heat flux distribution used by the coolant liquid; (ix) convective loss is neglected and (x) thermal resistance perpendicular to liquid–vapor interface is neglected.

It has been assumed that the nature of the meniscus in each corner is identical irrespective of its orientation. Body force is small compared to the force due to pressure jump at the interface of liquid and vapor (Suman et al., [25]). One corner of a section of a heat pipe of any polygonal shape of length Δx is taken as the control

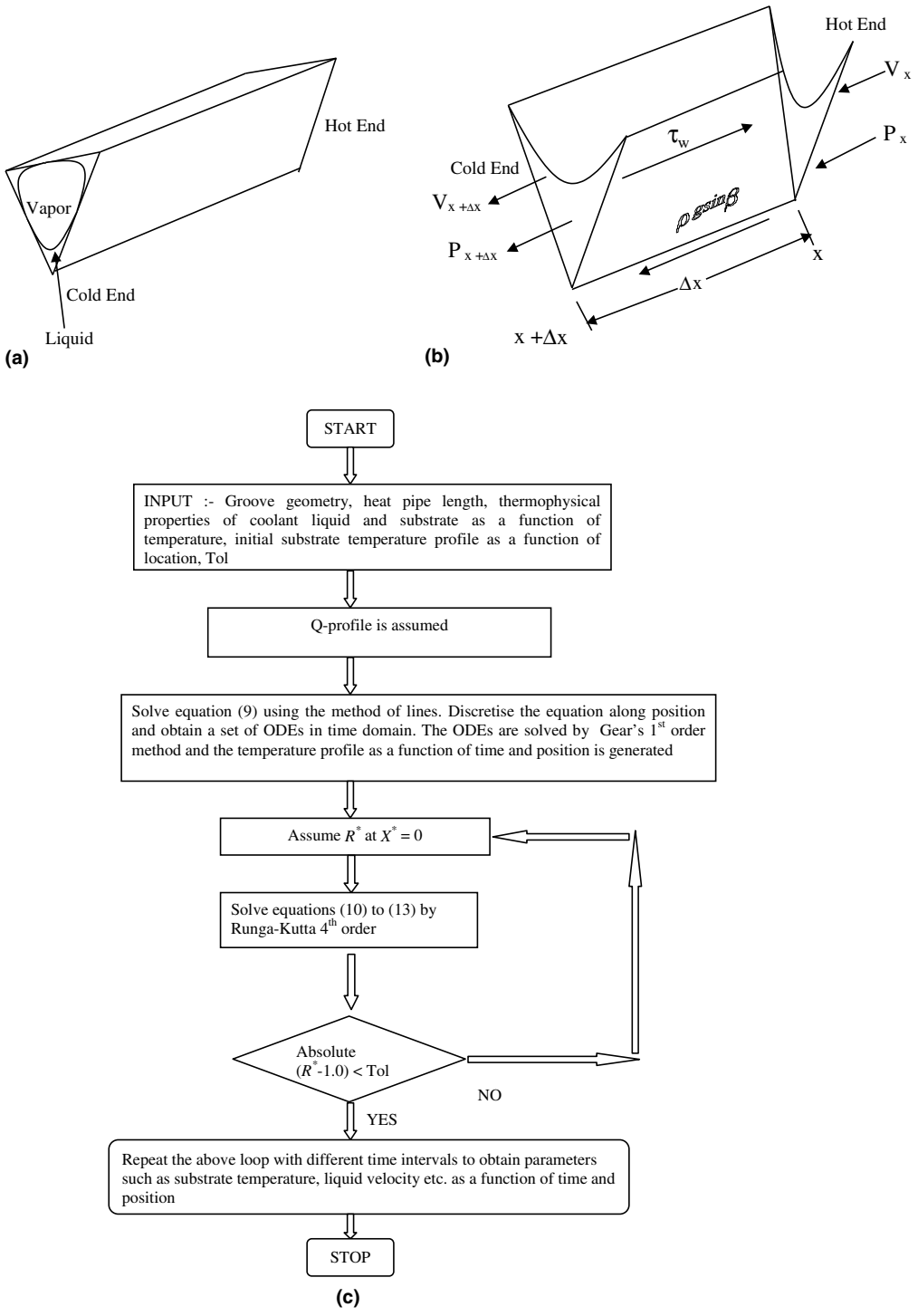

Fig. 1. (a) Schematic of the triangular micro-grooved heat pipe. (b) Schematic of a volume element with all forces specified. (c) Flow chart of the numerical technique.

volume and is shown in Fig. 1(b). The liquid pressure is a function of radius of curvature and the relationship is given by the Young–Laplace equation in the differential form,

$$\frac{\partial P_l}{\partial x} = \frac{\sigma_l}{R^2}\frac{\partial R}{\partial x} \tag{1}$$

The terms $\frac{\partial P_l}{\partial x}$ and $\frac{\partial R}{\partial x}$ are the pressure gradient and radius of curvature gradient, respectively. The unsteady state momentum balance in differential form is,

$$\rho_l A_l V_l \frac{\partial (V_l)}{\partial x} + A_l \frac{\partial P_l}{\partial x} + 2L_h \tau_w - \rho_l g \sin\beta A_l + \frac{\partial(\rho_l A_l V_l)}{\partial t} = 0 \tag{2}$$

The first term in the above equation represents the convective momentum change, the second term is the pressure force acting on the element, the third term represents the wall shear force, the fourth term is gravity force and the fifth term is the rate of accumulation of the convective momentum. The parameter A_l, signifying the liquid area at the corner depends on the number of corners and position, and is presented in the Appendix A.

At unsteady state, the difference between the mass entering and leaving the volume element is equal to the mass evaporated from that volume element and the mass accumulated in the control volume. Thus the differential form of the mass balance is,

$$\frac{\partial(\rho_l A_l)}{\partial t} + \frac{\partial(\rho_l A_l V_l)}{\partial x} + \frac{Q_v R_m}{\lambda_l} = 0 \tag{3}$$

The first term in Eq. (3) represents the rate of the accumulation of mass, the second term is the change of the liquid mass due to convection and the third term represents the mass of the liquid evaporated. R_m represents the meniscus surface area per unit length of the heat pipe and is presented in the Appendix A. All the terms in the above equation are functions of the radius of curvature (R) and therefore, vary along with the length of the heat pipe.

A part of the heat taken up by the coolant liquid is used to raise the temperature of the liquid while the remaining heat is used for evaporation and the accumulation of the heat as sensible heat in the control volume. Therefore, the unsteady energy balance equation in the differential element becomes,

$$\rho_l C_{pl} A_l \frac{\partial T_l}{\partial t} + \rho_l C_{pl} V_l A_l \frac{\partial T_l}{\partial x} - Q w_b + Q_v R_m = 0 \tag{4}$$

where Q is the heat flux taken up by the coolant liquid from the solid substrate.

Q is positive when taken up by the coolant liquid (in the evaporative section). It is negative when it is released by the coolant liquid (in the condenser region) to the substrate. It is zero in the adiabatic section, no evaporation and condensation take place in this region. The first term in Eq. (4) represents the rate of accumulation of sensible heat, the second term is the sensible heat rise of the element. The heat added (from outside) to the element is represented by the third term while the heat leaving the element by evaporation is given by the fourth term.

The unsteady state energy balance in the substrate is given by:

$$A_{cs} K_s \frac{\partial^2 T_S}{\partial x^2} - Q w_b - \rho C_{ps} A_{cs} \frac{\partial T_s}{\partial t} = 0 \tag{5}$$

where the first term is the net change in the conductive heat in the control volume, the second term is the heat taken up by the coolant liquid and the third term is the rate of accumulation of thermal energy in the control volume.

2.1. Initial and boundary conditions

The boundary conditions at the cold end ($x = L$):

$$R = R_0; \quad P_l = P_{v_0} - \frac{\sigma_l}{R_0}; \quad T_s = T_{Con} \quad \text{for all } t$$

R_0, the radius of curvature at the cold end is obtained from the groove geometry. The temperature at the end of the condenser region, T_{Con}, is taken to be 32 °C.

At the hot end ($x = 0$):

$$Q_{heater} = -K_s A_{cs} \left.\frac{\partial T_s}{\partial x}\right|_{x=0}; \quad V_l = 0; \quad \text{for all } t$$

The initial conditions:

$$\text{at } t = 0 \quad T_s = T_{Con}; \qquad V_l = 0;$$
$$P_l = P_{v_0} - \frac{\sigma_l}{R_0} - \rho_l g (L - x)\sin\beta;$$
$$R = \frac{\sigma}{(P_{v_0} - P_l)} \quad \text{for all } x$$

2.2. Non-dimensionalization

The Eqs. (1)–(5) are non-dimensionalized using the following parameters: friction factor, $f = K'/N_{Re}$, Reynolds number, $N_{Re} = D_h \rho_l V_l / \mu_l$, where, hydraulic diameter, $D_h = 4A_l/(2L_h)$, wall shear stress, $\tau_w = \rho V_l^2 f/2$ reference velocity, $V_R = Q'/(\rho_l R_0^2 \lambda_l)$, reference pressure, $P_R = \sigma_l/R_0$, reference temperature, $T_R = 32$ °C (ambient temperature, taken in this work), time constant, $\tau = \frac{K_s}{\rho_s C_{ps} L^2}$. The dimensionless parameters are defined as follows: R^* (dimensionless radius of curvature) = R/R_0; X^* (dimensionless position) = x/L; V^* (dimensionless liquid velocity) = V_l/V_R; P^* (dimensionless liquid pressure) = P_l/P_R; T_s^* (dimensionless substrate temperature) = T_s/T_R; T_l^* (dimensionless coolant liquid temperature) = T_l/T_R; t^* (dimensionless time) = $t\tau$. K' is used in the expression of the friction factor, f (Wu and Cheng [33]), and is a constant for a specific geometry. R_0 is the radius of curvature at the cold end and is a function of side length, the contact angle for the substrate and coolant liquid system and the apex angle of the polygon.

After non-dimensionalizing and rearranging, Eqs. (1)–(5) result into the following equations:

$$\frac{\partial R^*}{\partial X^*} = \frac{\left[\rho_l g \sin(\beta) + \frac{Q_v V_R R_m V^*}{A_l \lambda_l} - \frac{B_2 V_R V^*}{(R_0 R^*)^2} - \rho_l V_R \tau \frac{\partial V^*}{\partial t^*}\right]}{\left[\frac{\sigma_l}{R_0 L R^{*2}} - 2\rho_l \frac{V_R^2 V^{*2}}{L R^*}\right]} \tag{6}$$

$$\frac{\partial V^*}{\partial X^*} = -\left[\frac{Q_v R_m L}{\rho_l A_l \lambda_l V_R} + 2\frac{V^*}{R^*}\frac{\partial R^*}{\partial X^*} + \frac{2L\tau}{R^* V_R}\frac{\partial R^*}{\partial t^*}\right] \tag{7}$$

$$Q_V = \frac{1}{R_m}\left[Q w_b - \frac{\rho_l C_{pl} V_R V^* A_l T_R}{L}\frac{\partial T_l^*}{\partial X^*} - \rho_l C_{pl} A_l T_R \tau \frac{\partial T_l^*}{\partial t^*}\right] \tag{8}$$

$$\frac{\partial T_s^*}{\partial t^*} = \frac{\partial^2 T_s^*}{\partial X^{*2}} - \frac{Q w_b L^2}{T_R A_{cs} K_s} \tag{9}$$

$$\frac{\partial P^*}{\partial X^*} = \frac{\sigma_l}{R_0 P_R R^{*2}}\frac{\partial R^*}{\partial X^*} \tag{10}$$

In the formulation and non-dimensionalization of the governing equations, all transfer processes have been considered to be unsteady. The heat transfer by conduction is the slowest transfer process and it is assumed that this process will govern the transient behavior and other transfer processes can be treated at steady state. Therefore, the time derivatives of liquid velocity and radius of curvature have been neglected in Eqs. (6) and (7), respectively. The similar type of model reduction based on above assumption is available for asymmetrical flat-plate and disc-shape wicked heat pipe [26,29]. In Eq. (8), the sensible heat content terms are very small compared to the other two terms since other terms are related to two-phase heat transfer and the sensible heat content term is multiplied by A_l, which makes it even smaller. A similar conclusion is drawn by (Ravikumar and DasGupta [19]). Hence, the simplified governing equations (Eqs. (6)–(8)) can be written as,

$$\frac{\partial R^*}{\partial X^*} = \frac{\left[\rho_l g \sin(\beta) + \frac{Q_v V_R R_m V^*}{A_l \lambda_l} - \frac{B_2 V_R V^*}{(R_0 R^*)^2}\right]}{\left[\frac{\sigma_l}{R_0 L R^{*2}} - 2\rho_l \frac{V_R^2 V^{*2}}{L R^*}\right]} \tag{11}$$

$$\frac{\partial V^*}{\partial X^*} = -\left[\frac{Q_v R_m L}{\rho_l A_l \lambda_l V_R} + 2\frac{V^*}{R^*}\frac{\partial R^*}{\partial X^*}\right] \tag{12}$$

$$Q_V = \frac{1}{R_m}[Q w_b] \tag{13}$$

where A_l, W_b, R_m, B_2 and B_1 are defined in the Appendix A.

Eqs. (9)–(13) are valid for all the three regions of the heat pipe namely, evaporative, adiabatic and condenser. Q is zero in the adiabatic section. It is negative in the condenser region (heat is extracted) and is positive for the evaporative zone (heat is supplied). Linear and constant Q-profiles have been used in this study. For constant Q-profile, the heat flux is constant throughout the evaporator region and the effective input heat flux is 8×10^5 W/m^2. In the case of linear heat flux distribution, the maximum heat flux is at the beginning of the evaporator region and it reduces to zero at the junction of the evaporator and the adiabatic region. The heat flux at the liquid vapor interface is a function of time and position. These equations have been solved numerically taking predefined heat flux distribution i.e. Q-profile for the heat that is being transferred between the coolant liquid and the substrate. The dimensionless initial and boundary conditions are as follows: The boundary conditions:

at cold end $(X^* = 1),\ R^* = 1; \quad P^* = \frac{P_{v_0}}{P_R} - 1;$

$T_s^* = \frac{T_{Con}}{T_R}$ for all t^*

at hot end $(X^* = 0),\ Q_{heater} = -\frac{K_s A_{cs} T_R}{L}\left.\frac{\partial T_s^*}{\partial X^*}\right|_{X^*=0}$

$V^* = 0$ for all t^*

The initial conditions:

at $t^* = 0\ T_s^* = \frac{T_{Con}}{T_R}; \quad V^* = 0;$

$P^* = \frac{P_{v_0}}{P_R} - 1 - \frac{\rho_l g L(1 - X^*)\sin(\beta)}{P_R};$

$R^* = \frac{\sigma_l}{(P_{v_0} - P_R P^*) R_0}$ for all X^*

2.3. Numerical solution

The model equations (9)–(13) are a set of PDEs and algebraic equations. The model inputs are groove geometry, heat pipe length, Q profile and thermophysical properties of coolant liquid and substrate as a function of temperature. Eq. (9) has been solved using method of lines independently since it is decoupled from the other equations. The discretization of the equations is done along position and a set of ODEs in time domain has been obtained. The ODEs have been solved using Gear's 1st order method. The Gears 2nd order is also tried but significant change in result has not been observed. Gear's 1st order works well since its one-dimensional problem and the step size can freely be decreased to obtain stable result. The dimensionless step size of time is taken as 10^{-6} and step size for dimensionless length is 5×10^{-2}. With this step size, the results are found to be independent of step sizes.

Once the temperature profile is obtained as a function of position and time, Eqs. (10)–(13) have been

solved using Runga–Kutta 4th order integration techniques to obtain the radius of curvature, liquid velocity etc. as a function of position. They have been solved taking different temperature profiles for different times. The radius of curvature, liquid velocity etc, for a particular position at different values of time has been calculated and plotted against time to obtain the transient profiles. For Eqs. (10)–(13), boundary conditions for R^* and P^* at the hot end i.e., $X^* = 0$ are not known. The value of R^* at the hot end ($X^* = 0$) is assumed. P^* at the hot end i.e. $X^* = 0$ can be calculated since it is solely a function of the radius of curvature. Then Eqs. (10)–(13) are integrated from $X^* = 0$ to 1. R^* should be equal to 1 at the cold end ($X^* = 1$) as the cold end is completely filled with the coolant liquid. If the obtained value of R^* at the cold end is not equal to 1, a new value of R^* at the hot end is assumed and the integration process is repeated till the conditions $R^* = 1$ at $X^* = 1$ is achieved. The results produced are independent of step size and step size of 10^{-4} has been used. In this way, the transient profiles for substrate temperature, radius of curvature, liquid velocity etc., have been calculated. The computation flow chart describing the numerical approach in brief is shown in Fig. 1(c).

3. Results and discussion

The transient behaviors of a micro-grooved heat pipe have been studied by considering triangular groove though the developed model is capable of handling a heat pipe of any polygonal shape. The silicon substrate is 0.8 cm wide and 2.8 cm long. A portion of the length, 0.3 cm, is not grooved, which is used by the heater to supply the heat to the system. Hence, the effective length of the heat pipe is 2.5 cm. The lengths for the evaporative, the adiabatic and the condenser regions are assumed to be equal. The groove width and groove spacing are taken to be 0.2 mm. Ten such grooves have been considered. The temperature at the condenser end is taken as 32 °C and the angle of inclination is 10 °. A heat input of 2 W with linear and constant Q-profiles has been taken. For the constant Q-profile, the effective input heat flux is 8×10^5 W/m^2. Heat is given to the system with a heater and therefore, Q_{heater} is taken as equal to the heat input. In the case of linear heat flux distribution, maximum heat flux in the evaporative region is at the hot end and minimum heat flux in the condenser region is at the cold end. Pentane is taken to be the working fluid and silicon as the substrate. Pentane wets silicon completely i.e. γ (contact angle) is zero.

In Fig. 2(a), the substrate temperature is plotted as a function of time for different heat inputs at two different locations, $L/4$ and $3L/4$. $L/4$ and $3L/4$ are in the evaporative and condensing sections, respectively. It is found that lower the heat input, lower is the difference between

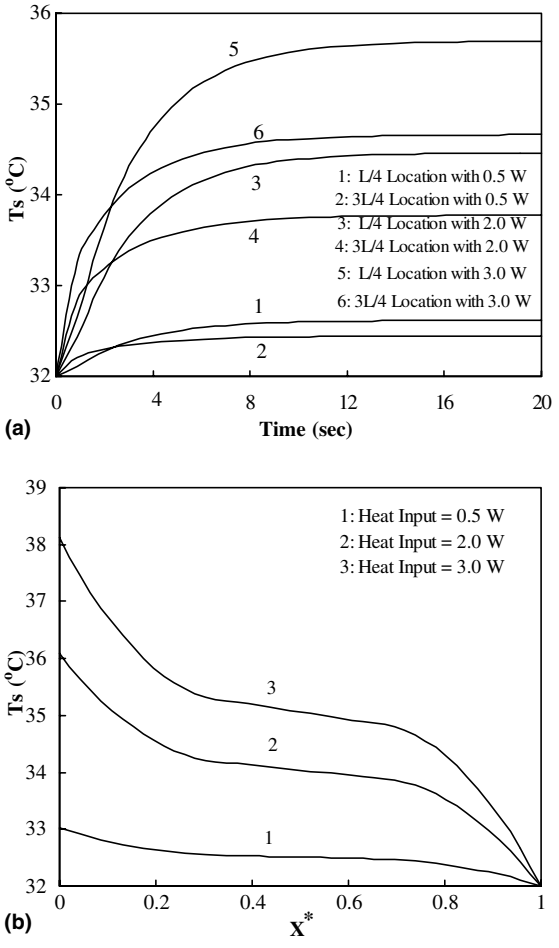

Fig. 2. (a) Variation of substrate temperature (°C) versus time (s) for different heat inputs with two different locations for triangular heat pipe (0.2 mm × 0.2 mm × 0.2 mm) with constant Q-profile. (b) Variation of the steady state substrate temperature (°C) versus dimensionless position for different heat inputs for triangular heat pipe (0.2 mm × 0.2 mm × 0.2 mm) with constant Q-profile.

the steady state and the initial temperature. The time required to reach the steady state increases with increase in the heat input value. They are found to be roughly 7.05 s and 11.30 s (Fig. 2(a)) for 0.5 W and 3.0 W, respectively. Fig. 2(b) is a steady state substrate temperature profile i.e. temperature as a function of location for different heat inputs. The temperature in the adiabatic region remains the same since there is no exchange of heat between the substrate and the coolant liquid. The temperature is decreasing in the evaporative and condenser regions with length. Heat is taken by the coolant liquid in the evaporative section and therefore, the substrate temperature profile is concave upward in this section. Heat is released by the coolant liquid in the condenser section and therefore, the substrate temperature

profile is convex upward in the condenser section. The slope of the temperature profile at the junction of evaporative and adiabatic regions is zero, since the amount of heat supplied to the substrate by the heater has been utilized by the coolant liquid in the evaporative region. It can be observed from the figure that the non-linearity of the substrate temperature increases with increase in the heat input value. Higher the heat input, larger is the temperature difference between initial and the steady state.

In Fig. 3(a), the transient profiles for substrate temperature at locations $L/4$ and $3L/4$ have been shown for different groove dimensions. The temperature difference between the initial and steady state is more for smaller groove dimension. It is clear from the figure that the time required to reach steady state is more for smaller groove dimension. In Fig. 3(b), the steady state substrate temperature profiles for different groove dimensions have been presented. It can be said that for smaller groove dimension, the temperature difference required to transfer the same amount of heat is more since the area available for heat transfer due to conduction is less for a groove with lower dimension. The area available for the heat conduction is $1.67 \times 10^{-5}\,m^2$ and $8.29 \times 10^{-5}\,m^2$ for groove dimensions of 0.1 mm and 0.5 mm, respectively.

In Fig. 4(a), the effect of Q-profiles on the substrate temperature profile as a function of time is presented. The linear and constant Q-profiles have been considered. It can be observed that from the figure that the difference between the initial and the steady state temperature is less with constant Q-profile than with linear one. It can be said that the time required for reaching the steady state for both Q-profiles are roughly the same. The

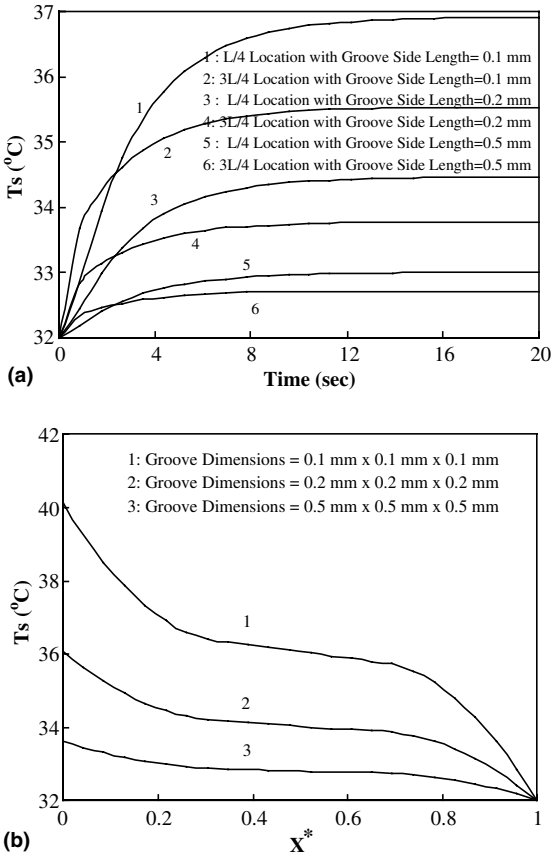

Fig. 3. (a) Variation of substrate temperature (°C) versus time (s) for different triangular groove dimensions with constant Q-profile. (b) Variation of the steady state substrate temperature (°C) versus dimensionless position for different locations for different triangular groove dimensions with constant Q-profile.

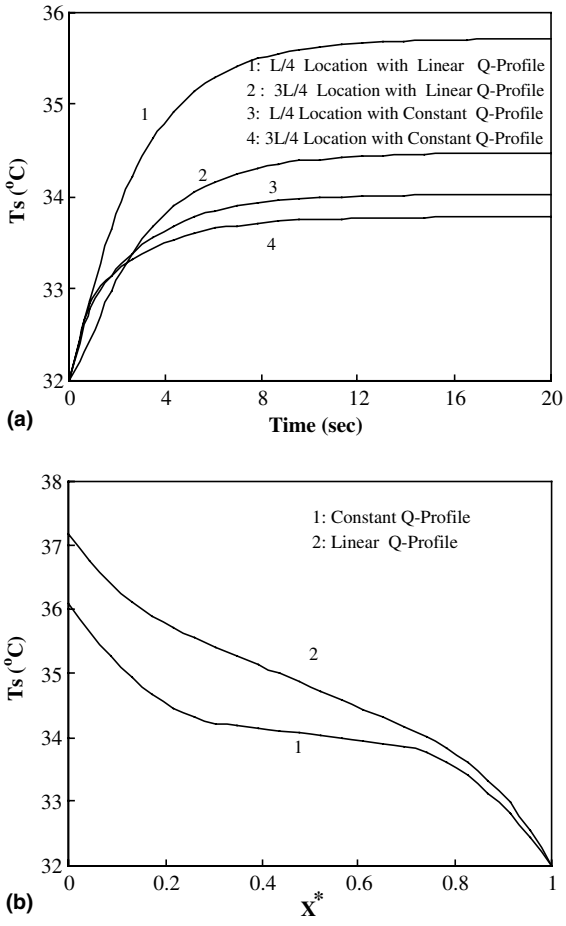

Fig. 4. (a) Variation of temperature (°C) versus time (s) for two different locations for different Q-profiles at two different locations for triangular micro-grooved heat pipe ($0.2\ mm \times 0.2\ mm \times 0.2\ mm$). (b) Variation of the steady state substrate temperature (°C) versus dimensionless position for two different Q-profiles for the triangular micro-grooved heat pipe ($0.2\ mm \times 0.2\ mm \times 0.2\ mm$).

steady state substrate temperature profiles for different Q-profiles are plotted in Fig. 4(b). From the figure, it is evident that the temperature profile for linear Q-profile is always higher than profile with constant Q-profile. The change of slope of the temperature profile with constant Q-profile is distinct at the juncture of evaporative and adiabatic sections. With linear Q-profile, the heat input itself goes to zero as evaporative section is about to end and therefore, there is not distinct change in slope at the juncture of evaporative and adiabatic sections has been observed.

The radius of curvature has an important role in the performance of micro-grooved heat pipes. In Fig. 5(a), the transient profile of the dimensionless radius of curvature at location, $X^* = 0.5$ is presented. The cold end is completely filled i.e., $R^* = 1$ at the cold end and the liquid pressure at the cold end can be evaluated. At $t = 0$, fluid inside the heat pipe is static and therefore, the liquid pressure along the length of heat pipe can be calculated. With the help of liquid and vapor pressures at $t = 0$, R^* at $t = 0$ has been evaluated. The transient behavior of radius of curvature is because of dependency of thermophysical properties of coolant liquid on temperature. Initially, the groove is optimally filled and therefore, radius of curvature is close to one, considering complete wetting principle. As the heater starts supplying the heat to the substrate, the coolant liquid starts evaporating in the evaporative section and it starts condensing in the condenser section. Result is that the liquid poor starts depressing and the radius of curvature starts decreasing in the evaporative section. The radius of curvature is one at the cold end and the difference in radius of curvature between the evaporative and condenser sections generates the driving force for the liquid pool to move towards the evaporative zone. Once the driving force generated by the change in radius of curvature is able to pump necessary amounts of the coolant liquid required for evaporation in the evaporating section, the radius of curvature reaches its steady state. The time needed to reach steady state is within 10 s for all the cases studied herein. If the amount of heat taken up by the substrate to increase its sensible heat is taken into account i.e. removing assumption (iv), qualitatively the same conclusion for variations in radius of curvature and liquid velocity (discussed in next section) will be drawn since the input heat to the heat pipe will be less and therefore, the radius of curvature will decrease from close to one value (its initial value) to the steady state value. The steady state profile of the dimensionless radius of curvature along the length of the heat pipe is shown in Fig. 5(b). The value of the radius of curvature at the cold end is more and at the hot end is less. The variation of radius of curvature along the length of the heat pipe provides the necessary driving force for the capillary pumping required for steady flow from the cold end to the hot end.

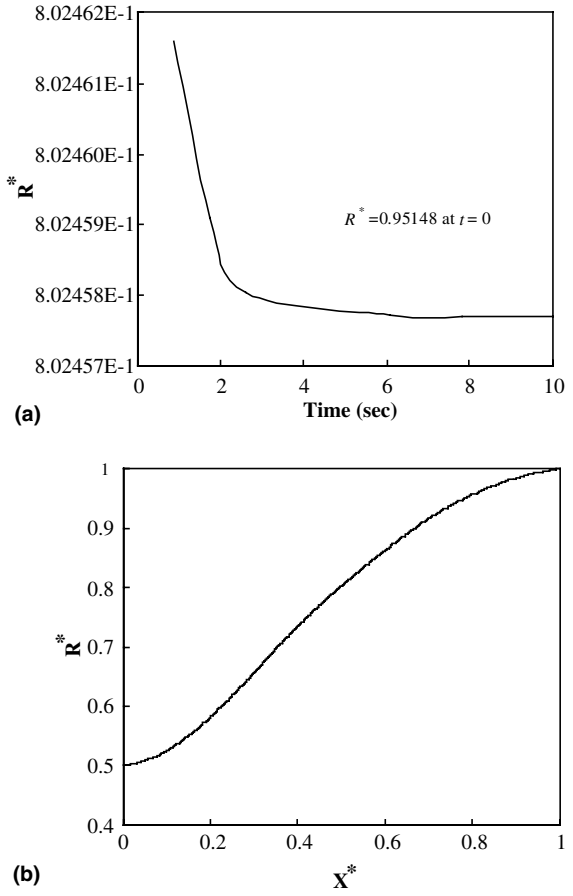

Fig. 5. (a) Variation of dimensionless radius of curvature at $L/2$ location versus time (s) for a triangular micro-grooved (0.2 mm × 0.2 mm × 0.2 mm) heat pipe with constant Q-profile and 0.02 W heat input. (b) Variation of the steady state dimensionless radius of curvature versus dimensionless position, X^* for a triangular micro-grooved (0.2 mm × 0.2 mm × 0.2 mm) with constant Q-profile and 0.02 W heat input.

In Fig. 6(a), the transient profile for liquid velocity at location, $X^* = 0.5$ is presented. At $t = 0$, fluid inside the heat pipe is static and therefore, $V^* = 0$ at $t = 0$. The direction of flow of coolant liquid is from the cold end to the hot end. Initially, the liquid pool is at rest and once the evaporation starts and liquid starts flowing towards the hot end. The driving force for the fluid flow is generated due to change in the change in the radius of curvature with position. The liquid velocity keeps increasing till the fluid flow meets the evaporation requirement at the evaporative section and then it reaches its steady state value. It can be seen that the liquid velocity reaches its steady state value within 10 s. The transient behavior in liquid velocity is also affected by the dependency of thermophysical properties on temperature. The steady state profile of the liquid velocity

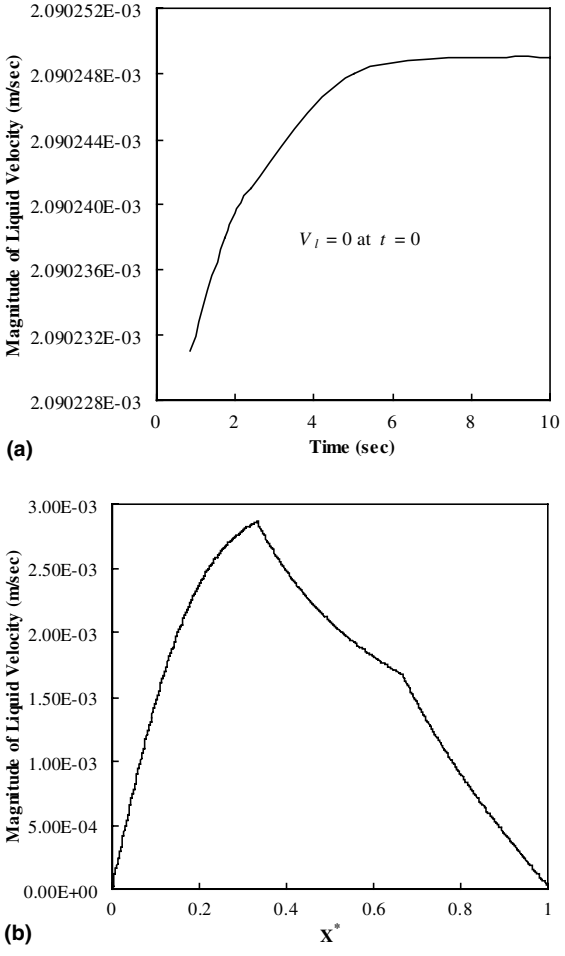

Fig. 6. Variation of magnitude of liquid velocity (m/s) at $L/2$ location versus time (s) for a triangular groove (0.2 mm × 0.2 mm × 0.2 mm) with constant Q-profile and 0.02 W heat input. (b) Variation of magnitude of the steady state liquid velocity (m/s) versus dimensionless position, X^* for a triangular groove (0.2 mm × 0.2 mm × 0.2 mm) with constant Q-profile and 0.02 W heat input.

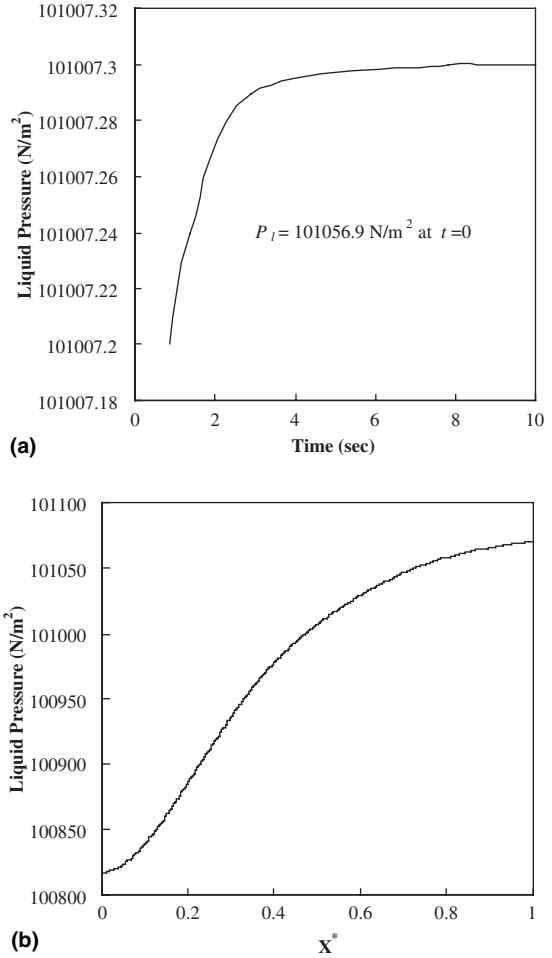

Fig. 7. (a) Variation of magnitude of liquid pressure (N/m^2) at $L/2$ location versus time (s) for a triangular groove (0.2 mm × 0.2 mm × 0.2 mm) with constant Q-profile and 0.02 W heat input. (b) Variation of magnitude of the steady state liquid pressure (N/m^2) versus dimensionless position, X^* for a triangular groove (0.2 mm × 0.2 mm × 0.2 mm) with constant Q-profile and 0.02 W heat input.

along the length of the heat pipe is shown in Fig. 6(b). It may be observed from the figure that liquid velocity increases in the evaporative section. This is due to the cumulative effect of replenishing the amount evaporated throughout the evaporation region. It decreases moderately in the adiabatic section. This is because of increase in liquid area and the loss due to friction factor. It sharply decreases in the condenser region.

In Fig. 7(a), the transient profile for liquid pressure at location, $X^* = 0.5$ has been presented. The cold end is completely filled i.e., $R^* = 1$ at the cold end and the liquid pressure at the cold end can be evaluated. At $t = 0$, fluid inside the heat pipe is static and therefore, the liquid pressure along the length of heat pipe can be calculated. Once the evaporation starts, the radius of curvature and the temperature of the coolant liquid start changing with position and liquid pressure start changing. The transient liquid profile is increasing with time because the effect of variation in surface tension on the liquid pressure is more than the effect of variation in radius of curvature on liquid pressure. The variation in radius of curvature is small because the transient behavior in radius of curvature is only due to dependency of thermophysical properties on temperature. If the sensible heat taken by the substrate is considered, the variation in radius of curvature will be more and that will result in decrease in the transient liquid pressure. It is clear from this work as well since initial liquid pressure is

more than its steady state value. The difference in liquid pressure between the evaporative and condenser sections is the driving force for the fluid flow. It reaches its steady state value within 10 s. The transient behavior in liquid pressure is because of the dependency of thermophysical properties on temperature. In Fig. 7(b), the steady state liquid pressure has been presented. The steady state liquid pressure is the direct outcome of the radius of curvature. The equation relating these parameters i.e. Eq. (10) suggests that the trend for radius of curvature and the liquid pressure should be the same. The presented liquid pressure profile is of similar nature that of radius of curvature.

In the study by Anand et al. [23], experiments were carried out in a specially designed cell to study the onset and the propagation of dry out point on a micro-grooved silicon surface with pentane as the coolant liquid. Chemical machining method was used to fabricate V-shaped axial micro-grooves on a silicon substrate. Controlled heat was supplied to the top of the substrate and axial temperature distribution was accurately measured as a function of input heat and inclination of the substrate to the horizontal. The comparison between the dry (without liquid) and wet (with liquid) temperature profiles was used to locate the dry-out point and its propagation as a function of inclination angle and supplied heat flux. 33 V-grooves of 2 cm length with groove depth of 68.82 μm, groove width of 100 μm and a groove pitch of 200 μm were used. Pentane was used as the coolant. A resistance heater was used as the source of heat and the backside of which was carefully insulated to ensure that all of the supplied heat went into the system. Careful design of the system excluded the possibility of any vapor loss from the system. A series of small thermocouples accurately measured the temperature profiles as functions of heat input to the system and inclination angle. The steady state substrate temperature profile for this system is calculated for a heat input of 1.52 W and 1.31 W with inclination of 14.93° and 43.16°, respectively. The convective loss is neglected, as it is small compared to the two-phase heat transfer. The comparison of calculated and experimental temperature profile is presented in Fig. 8. The figure shows reasonable agreement between the experimental and the theoretical predictions. The maximum discrepancy is in the adiabatic section though less than 7%. The possible causes of this discrepancy are as follows. Firstly, the heat flux taken up by the liquid is assumed to be constant, which may be in error. However, the exact nature of the distribution cannot be determined without taking recourse of the experimental data [23], thereby compromising the independent nature of the developed theoretical model. Secondly, neglecting the convective losses can also result in the over-prediction of temperature. However, the generalized model, based on first principle, proposed in this study, correctly predicts the behavior of micro-groove heat pipes in terms of trends in radius of curvature, axial liquid velocity and pressure and satisfactory agreement with the experimental results for substrate temperature of a previous study.

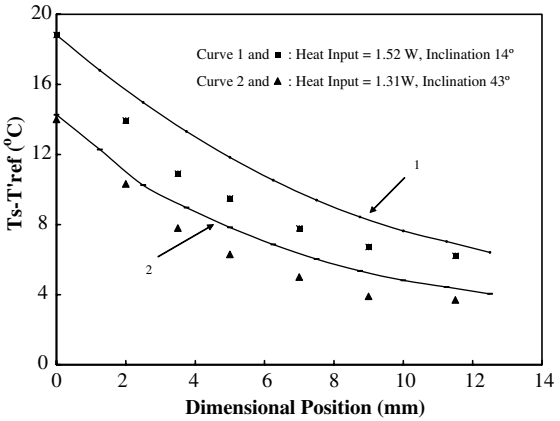

Fig. 8. Comparison of the theoretical and experimental (Anand et al. [23]) steady state substrate temperature profiles. The points are the experimental data and the solid lines are theoretical predictions.

4. Summary and conclusion

A transient model for a micro-grooved heat pipe of any polygonal shape is presented using a macroscopic approach. The triangular micro-heat pipe has been taken as a test case. The coupled equations of heat, mass and momentum transfer are solved to obtain the transient as well as the steady state profiles of various parameters namely, the substrate temperature, the liquid velocity, the liquid pressure, etc. The time required to reach the steady state for the substrate temperature is found to be less than 20 s. The time required is more for higher heat load and smaller substrate area. The obtained results give a qualitative description of the transient phenomena in the fluid flow and mass transfer processes as well. The transient profile for radius of curvature is decreasing with time and reaches steady state within 10 s. The transient profiles for liquid velocity and liquid pressure are increasing with time and reach steady state within 10 s. The steady state for substrate temperature results are successfully compared with the experimental results available in the literature.

Acknowledgement

This work is supported by a grant from BRNS, Government of India, under the scheme no. 2001/36/12/BRNS/726. Any opinion, findings and conclusions or recommendations expressed in this paper are those of

the authors and do not necessarily reflect the views of BRNS.

Appendix A

For polygonal heat pipe with equal sides:

$$R_0 = \frac{a \sin \alpha}{2 \cos(\alpha + \gamma)}$$

where a is side length of the polygon or smaller side of rectangle

$$Q = 3Q'/naL$$

where, Q' is the heat input per channel and Q is the heat flux.

$$\alpha = (n-2)\pi/2n$$

where α is half apex angle and n is the number of sides of the polygon

$$W_b = na$$

where W_b is groove pitch.

For the rectangular heat pipe (side ratio 1:2):

$$R_0 = \frac{a \sin \alpha}{2 \cos(\alpha + \gamma)}$$

$$Q = 3Q'/2(a + a_1)L$$

where a_1 is the larger side of rectangle.

$$\alpha = \pi/4$$

$$W_b = 2(a + a_1)$$

For the triangular (equilateral) heat pipe:

$$n = 3$$

$$R_0 = \frac{a \sin \alpha}{2 \cos(\alpha + \gamma)}$$

$$W_b = na$$

$$Q = 3Q'/(W_b L)$$

$$\alpha = \pi/6$$

Geometry of one corner of the polygonal heat pipe is presented in Fig. A1.

The shaded area in Fig. A1 is the cross-sectional area of the liquid in the heat pipe. The cross-section area of one corner is expressed as:

$$A_l' = \text{area of ACBD} + \text{area of } \Delta ABC - (\text{area of sector AOB} - \text{area of } \Delta AOB)$$

The line diagram of section OBC in Fig. A1 is presented in Fig. A2 in detail.

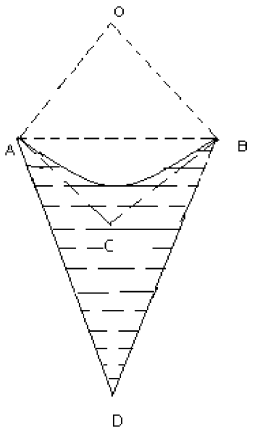

Fig. A1. Geometry of a liquid filled corner.

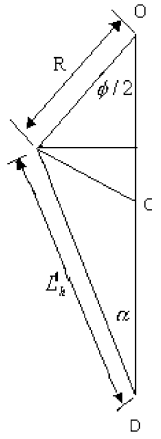

Fig. A2. Line diagram of section OBC in Fig. A1.

From Fig. A2,

AC and BC are the tangents to the liquid meniscus.

$$\angle CAD = \gamma$$
$$\angle ADC = \alpha$$
$$\angle ACB = 2(\alpha + \gamma)$$
$$\angle AOB = \phi = \pi - 2(\alpha + \gamma)$$

$$R_0 = \frac{a \sin \alpha}{2 \cos(\alpha + \gamma)}$$

$$L_h' = R \frac{\cos(\alpha + \gamma)}{\sin \alpha}$$

$$L_h = nL_h'$$

$$R_m = nR\phi$$

$$\text{Area of ACBD} = \frac{R^2 \cot(\alpha + \gamma) \cos(\alpha + \gamma) \sin \gamma}{\sin \alpha}$$

$$\text{Area of } \Delta ABC = R^2 \cot(\alpha + \gamma) \cos^2(\alpha + \gamma)$$

Area of sector $AOB = \phi R^2/2$

Area of $\Delta AOB = R^2 \cos(\alpha+\gamma)\sin(\alpha+\gamma)$

Hence,

$$A_1' = R^2\left[\{\cot(\alpha+\gamma) - \varphi/2\} + \frac{\cot(\alpha+\gamma)\cos(\alpha+\gamma)\sin\gamma}{\sin\alpha}\right]$$

and

$$\begin{aligned} A_1 &= nA_1' \\ &= nR^2\left[\{\cot(\alpha+\gamma) - \varphi/2\} + \frac{\cot(\alpha+\gamma)\cos(\alpha+\gamma)\sin\gamma}{\sin\alpha}\right] \\ &= B_1R^2 \end{aligned}$$

where

$$B_1 = n\left[\{\cot(\alpha+\gamma) - \varphi/2\} + \frac{\cot(\alpha+\gamma)\cos(\alpha+\gamma)\sin\gamma}{\sin\alpha}\right]$$

$$B_2 = \frac{\mu_l K' \cos^2(\alpha+\gamma)}{2\sin^2\alpha\left[\frac{\cot(\alpha+\gamma)\cos(\alpha+\gamma)\sin\gamma}{\sin\alpha} + \{\cot(\alpha+\gamma) - \varphi/2\}\right]^2}$$

References

[1] T.P. Cotter, Principles and prospects of micro-heat pipes, in: Proceedings of the 5th International Heat Pipe Conference, Tsukuba, Japan, 1984, pp. 328–332.

[2] L.W. Swanson, G.C. Herdt, Model of the evaporative meniscus in a capillary tube, J. Heat Transfer 114 (1992) 434–441.

[3] S. DasGupta, J.A. Schonberg, I.Y. Kim, P.C. Wayner Jr., Use of augmented Young–Laplace equation to model equilibrium and evaporation extended menisci, J. Colloid Interf. Sci. 157 (1993) 332–342.

[4] S. DasGupta, J.A. Schonberg, P.C. Wayner Jr., Investigation of an evaporative extended meniscus based on the augmented Young–Laplace equation, J. Heat Transfer 115 (1993) 201–208.

[5] M.L. Gee, T.W. Hearly, L.R. White, Ellipsometric studies of alkenes adsorption on quartz, J. Colloid Interf. Sci. 131 (1) (1989) 18–23.

[6] S. Gokhale, J.L. Plawsky, P.C. Wayner Jr., S. DasGupta, Experimental measurement of pressure gradient and fluid flow in a small spreading drop during condensation, Phys. Fluids 16 (6) (2004) 1942–1955.

[7] S. Moosman, S.M. Homsy, Evaporating menisci of wetting fluids, J. Colloid Interf. Sci. 73 (1980) 212–223.

[8] F. Renk, P.C. Wayner Jr., An evaporating ethanol meniscus; Part II: analytical studies, J. Heat Transfer 101 (1979) 55–62.

[9] J.G. Troung, P.C. Wayner Jr., Effects of capillary and Vander Waals dispersion forces on the equilibrium profile of a wetting liquid: theory and experimental, J. Chem. Phys. 87 (1987) 4180–4188.

[10] P.C. Wayner Jr., The effect of interfacial mass transport on flow in thin liquid films, Colloids Surf. 52 (1991) 71–84.

[11] P.C. Wayner Jr., Y.K. Kao, L.V. LaCroix, The interline heat transfer coefficient of an evaporative wetting film, Int. J. Heat Mass Transfer 19 (1976) 487–492.

[12] L. Zheng, J.L. Plawsky, P.C. Wayner Jr., S. DasGupta, Stability and oscillations in an evaporating corner meniscus, J. Heat Transfer 126 (2004) 169–178.

[13] B.R. Babin, G.P. Peterson, D. Wu, Steady state modeling and testing of a micro-heat pipe, J. Heat Transfer 112 (1990) 595–601.

[14] D. Wu, G.P. Peterson, Investigation of the transient characteristics of a micro-heat pipe, J. Thermophys. Heat Transfer 5 (1991) 129–134.

[15] G.P. Peterson, H.B. Ma, Theoretical analysis of the maximum heat transport in triangular grooves: a study of idealized micro-heat pipe, J. Heat Transfer 118 (1996) 731–739.

[16] D. Khrustalev, A. Faghri, Thermal analysis of a micro-heat pipe, J. Heat Transfer 116 (1) (1994) 189–198.

[17] X. Xu, V.P. Carey, Evaporative from microgroove surface—an approximate heat transfer model and its comperization with experimental data, J. Thermophys. Heat Transfer 4 (1990) 512–520.

[18] P.C. Stephan, C.A. Busse, Analysis of heat transfer coefficient of grooved heat pipe evaporator walls, Int. J. Heat Mass Transfer 35 (1992) 383–391.

[19] M. Ravikumar, S. DasGupta, Modeling of evaporation from V-shaped microgrooves, Chem. Engng. Commun. 160 (1997) 225–248.

[20] H.B. Ma, G.P. Peterson, Experimental investigation of the maximum heat transport in triangular grooves, J. Heat Transfer 118 (1996) 740–746.

[21] A.Md. Khan, S. Mishro, S. De, S. DasGupta, An experimental and theoretical investigation of evaporating cooling from V-shaped microgrooves, Int. J. Transport Phenom. 1 (1999) 277–289.

[22] J.M. Ha, G.P. Peterson, Analytical prediction of axial dry-out point for evaporating liquids in axial microgrooves, J. Heat Transfer 120 (1998) 452–457.

[23] S. Anand, S. De, S. DasGupta, Experimental and theoretical study of axial dry-out point for evaporative from V-shaped microgrooves, Int. J. Heat Mass Transfer 45 (2002) 1535–1543.

[24] I. Cotton, G.R. Stores, A semi-analytical model to predict the capillary limit of heated inclined triangular capillary grooves, J. Heat Transfer 124 (2002) 162–168.

[25] B. Suman, S. De, S. DasGupta, Modeling of the capillary limit of a micro groove heat pipe and the prediction of dry out length. Accepted for publication in International Journal of Heat and Fluid Flow, 2004.

[26] W.S. Chang, G.T. Colwell, Mathematical modeling of the transient operation characteristics of a low temperature heat pipe, Numer. Heat Transfer 8 (1985) 169–186.

[27] A. Faghri, M.M. Chen, A numerical analysis of the effects of conjugate heat transfer, vapor compressibility, and viscous dissipation in heat pipe, Numer. Heat Transfer A 16 (1989) 389–405.

[28] J.M. Turnier, M.S. El-Genk, A heat pipe transient analysis model, Int. J. Heat Mass Transfer 37 (1994) 753–762.
[29] N. Zhu, K. Vafai, Analytical modeling of startup characteristics of asymmetric flat-plate and disc-shaped heat pipes, Int. J. Heat Mass Transfer 41 (17) (1998) 2619–2637.
[30] J.M. Doster, M.L. Hall, Numerical modeling of high-temperature liquid metal heat pipes 1989 Joint ASME/AICHE. National Heat Transfer Conference, Philadelphia, Pennsylvania, 89-HT-13, 1–9.
[31] G.T. Colwell, W.S. Chang, Measurement of transient behavior of a capillary structure under the heavy thermal loading, Int. J Heat Mass Transfer (1983).
[32] W.S. Chang, Heat pipe start up from the supercritical state, Ph.D. desertion, School of Mechanical Engineering, Georgia Institute of Technology, 1981.
[33] H.Y. Wu, P. Cheng, Friction factor in smooth trapezoidal silicon microchannels with different aspect ratios, Int. J. Heat Mass Transfer 46 (2003) 2519–2525.